

An Automated 3D Turbomachinery Design and Optimization System

Dr. Ahmed F. Nemnem
Dept. of A/C Engineering
Military Tech. College
Cairo, Egypt
nemnemam@mail.uc.co
m

Prof. Mark G. Turner
Aerospace Engineering
Dept.
University of Cincinnati
Cincinnati, OH, USA
turnermr@ucmail.uc.edu

Kiran Siddappaji
Aerospace Engineering
Dept.
University of Cincinnati
Cincinnati, OH, USA
starays001@gmail.com

Prof. Anthony J. Gannon
Turbopropulsion Laboratory
Naval Postgraduate School
Monterey, California, USA
ajgannon@nps.edu

Abstract—An automated turbomachinery design and optimization system is introduced. An existing splintered transonic fan is used as a test case. The flow path and the geometrical properties of the rotor are initially created using one dimensional and axi-symmetric design analysis code. The blades are parametrically designed using a three dimensional blade geometry builder (3DBG) which includes a large design space with few parameters. The solid model creation of the rotor sector with periodic boundaries is automated using MATLAB code directly connected to SolidWorks. A mechanical optimization is performed using ANSYS Static Structural Module to ensure the blade(s) meets the given strength constraints with mass minimization. Once accepted, a CFD optimization is performed to evaluate efficiency and stall margin objective functions.

Keywords—Turbomachinery; Optimization; Design; Transonic; fan.

I. INTRODUCTION

Engine design is an iterative, multidisciplinary and complex process. The success of an engine design process depends on a carefully balanced design that best exploits and considers the interactions among the numerous traditional engineering disciplines such as aerodynamics and structures, as well as manufacturing. Turbofan engines are the most widely used engines in commercial and military applications. In commercial high bypass turbofan engines, the fan provides around 80% of the net thrust of the engine. In military low bypass mixed turbofan engines, the fan provides good pressure boosting at the inlet as well as cooling with sufficient fresh air for the afterburner. Designing a highly efficient, wide stall margin, fan system is considered an important goal through the detailed design phase. Fan blade detailed design is challenging. The design space for the fan can be increased by exploring tandem and splintered designs. By making the geometry definition parametric, a large design space can be explored efficiently.

Optimization is a process that iterates through the design steps, changing different parameters to minimize a defined objective function. The optimization process is useful in studying the effect of different parameters over the design space. Fan optimization

can be performed over one or multiple design steps. Creation of a single fan optimization loop that includes all the design steps is a challenging goal and needs to be carefully handled.

II. MOTIVATION

The recent progress in Multidisciplinary Optimization (MDO) enables engineers to revise design strategies and to address more complex problems. Design and optimization of a transonic fan is considered one of these complex problems. The common objective is found to be maximizing the efficiency range and total pressure ratio from an aerodynamic point of view (or constraining the pressure ratio).

Benini [1] optimized NASA rotor 37 to maximize both the isentropic efficiency and the pressure ratio at the design point while constraining the mass flow rate ($\frac{\dot{m}}{\dot{m}_{choke}} = 0.98$). He did a comparison of the Mach number contours near the suction surface for the three blades. In the original configuration, a strong normal shock wave occurred within the blade passage and led to high aerodynamic losses and severe shock/boundary-layer interaction. In both the E-O (efficiency objective) and PR-O (pressure ratio objective) blades, the shock bifurcated into two less severe branches and almost vanished into two shock/boundary-layer interaction zones.

Jang et al. [2] optimized NASA rotor 37 by maximizing the adiabatic efficiency using blade sweep. By optimizing the blade sweep of the rotor blade, the adiabatic efficiency was increased by 1.25% as compared to that of the reference shape. Jang found that the optimum shape improves the efficiency mainly in the middle of the span. The increase in adiabatic efficiency for the optimized blade is caused by moving the separation line downstream of the blade suction surface.

Lian and Liou [3] optimized NASA rotor 67 to maximize the stage pressure ratio and minimize the compressor weight using a genetic algorithm, gradient-based method, and response surface model. They made a comparison between the maximum pressure ratio design and baseline at 10, 50 and 90% span from the hub. At 10% span, the high-pressure ratio design has a larger camber but less thickness than the original design which means less weight. The difference in the pressure distribution is rather small.

The same conclusion was found to be true at 50% span. At 90% span, the high-pressure ratio design has a slightly smaller camber and thinner airfoil than rotor 67 blades. The pressure difference is rather large, indicating that transonic flow is sensitive to the shape change. They demonstrated 1.8% improvement in pressure ratio and 5.4% reduction in weight when applying the gradient-based method after the Genetic Algorithm (hybrid approach) which accelerates the optimization convergence rate.

Ellbrant et al. [4] presented optimization with a trade-off between high stall margin at low speed and high efficiency at high speed. The design method is based on an automatic multi-objective optimization process in 2 steps, 2D blade profile optimization considering both efficiency and stall margin then 3D stacking optimization.

The pressure loss ($\bar{\omega}$) in the relative frame is used as the objective for measuring efficiency. The static pressure recovery coefficient (C_p) is used to indicate the compressor stall margin at the design point (95.6 % full speed) based on part speed (55 % full speed). That is because, as rotor speed increases, its operating range decreases and so does its stability. Having a wide range of operation at a part speed allows the rotor to be stable at the off-design operations.

The objective functions were chosen as follows,

$$\begin{aligned} \text{Minimize: } f_1(x) &= \bar{\omega} \\ \text{Maximize: } f_2(x) &= C_p \end{aligned} \quad (1)$$

where $\bar{\omega}$ and C_p are the pressure losses and static pressure recovery coefficient respectively and they are defined in Ellbrant reference [4] as follows,

$$\begin{aligned} \bar{\omega} &= \frac{P_{02} \text{isen} - P_{02}}{P_{01} \text{rel} - P_1} \\ C_p &= \frac{P_2 - P_1}{P_{01} \text{rel} - P_1} \end{aligned} \quad (2)$$

where, P denotes the static pressure and P_o denotes the total pressure.

Quasi 3D and full 3D Pareto Front optimization were used. It was found that there is a gap between both results which is especially large when it comes to predict the lower radial spans of the blade due to the large difference in radius from inlet to outlet. It was found that new designs have not demonstrated a noticeable increase in efficiency at the design point compared to the original design. But at part speed, there was a significant increase in the stall margin relative to the original design which was accomplished through the 2D optimization.

The next year, Ellbrant et al. [5] had the same trade off but used a 3D RANS (Reynolds Averaged Navier–Stokes) solver in the first optimization level that reduced the analysis complexity from 3D to quasi 3D which allow exploring larger design space. Objective functions were stated to be polytropic efficiency (η_p) and static pressure recovery coefficient (C_p),

$$\begin{aligned} \text{Minimize: } f_1(x) &= \eta_p \\ \text{Maximize: } f_2(x) &= C_p \end{aligned} \quad (3)$$

In the presented work, a single fan optimization loop that includes all the design steps is demonstrated. Each structural and aerodynamic optimization loop results in an optimized design that once is done, it goes to the next optimization step. Eliminating the user from the loop is not recommended to decide a better design point and minimize the overall optimization time. The design and optimization processes allow a parametric design (sectional) to be able to transform the final optimized design in an iterative process from hot (operating design) to cold (manufactured design).

III.PROCESS OVERVIEW

The free open source DAKOTA program [6] from the Sandia National Laboratories is used for optimization. DAKOTA (Design Analysis Kit for Optimization and Terascale Applications) provides a flexible, extensible interface between analysis codes and iterative systems analysis methods. It works in parallel with many optimization options and it runs under Linux, Unix & Linux like environments (Windows with Cygwin)

Fig. 1 shows the general flow chart for the Dakota optimization process.

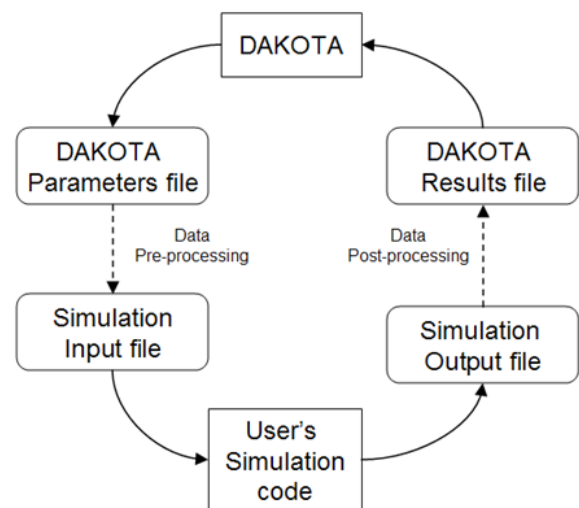


Fig. 1. Dakota flow chart.[6]

The full process is described as predefining the initial geometry parameters to create the initial 3D hot shape. A 3DBGB geometry generator [7] has been developed to define the blade design. Earlier versions had been discussed by Siddappaji [8]. The latest version had been developed with new features that allow for curvature control [9]. It is available online at (<http://gtsl.ase.uc.edu/3DBGB/>) as an executable.

The 3D solid is created using SolidWorks considering the fillet and tip clearance and the blades mass are evaluated. A structural analysis problem is constructed to evaluate the maximum rotor stress and constrain it to a safe percentage of the material ultimate tensile strength. Maximum stresses are calculated according to the centrifugal loads. The optimization process takes place until the maximum rotor stress is reduced and the blade mass is minimized. Only parameters that affect the strength and blades mass are varied during this part of the

process. These include the blades thickness and chord. The Mechanical optimization process is shown in Fig. 2,

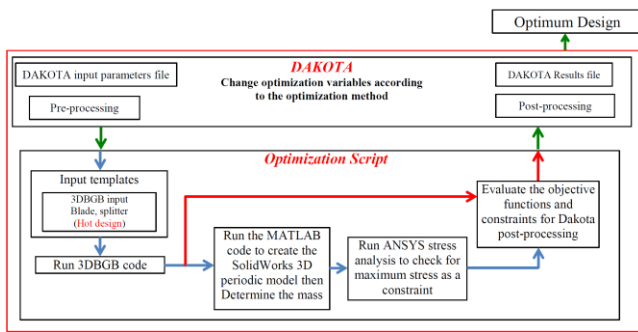


Fig. 2. Detailed Flow chart for the optimization process.

The CFD analysis is performed using the FINE/Turbo flow-solver [10]. The CFD case is constructed using the mechanically optimized hot shape to create the flow optimization problem. The maximization of the efficiency and/or stall margin are the objectives. Stall Margin investigation provides a measure of how close an operating point is to stall. Stability measure (Stall margin Range) is highly affected by different optimization techniques [4]. Keeping track of pressure ratio and mass flow rate allow using them as a constraint to obtain the optimum for a specific design point. The CFD optimization process for efficiency and/or stall margin is shown in Fig. 3,

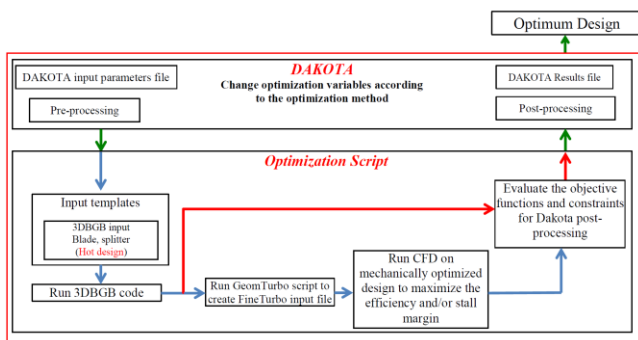


Fig. 3. Detailed Flow chart for CFD optimization process.

The objective function(s) and constraints are listed as follows:

1. Minimization of the mass of the blades
2. Minimization of $(1 - \eta_p)$ at 100% speed which will maximize stage efficiency (η_p)
3. Minimization of $(-C_p)$ at part speed (60%) which will maximize the pressure recovery factor (that estimates the stall margin) which was defined by Ellbrant et. al. [4], [5] as the attainable static pressure.

Each optimization is done independently and the result is transferred to the next step until reaching the optimum design. Connecting scripts have been developed to allow different run modes. The structural and aerodynamic analysis can be done in every iteration using a special script as shown in the flow

chart in Fig. 4, although will be a time consuming optimization.

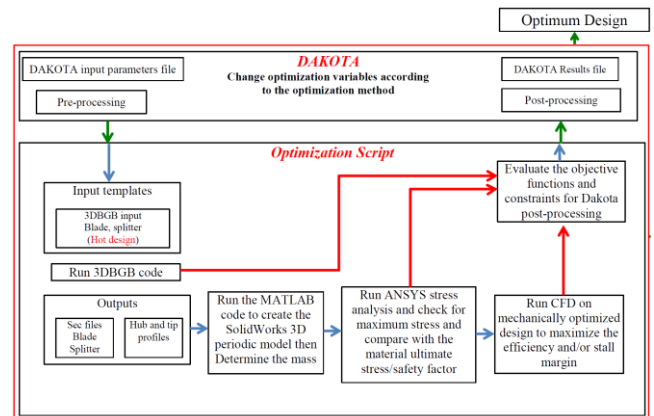


Fig. 4. Detailed Flow chart for the whole optimization process.

IV. INITIAL DESIGN

A transonic fan optimization is considered as a test case. A transonic fan with a splitter was designed by Scott Drayton in 2013 [11] at the Naval Postgraduate School (NPS). An optimization system that explored the design of a novel, but operating design would be general and more functional than using a more conventional configuration. The rotor contains 24 blades oriented in periodic order with 12 main blades and 12 splitters. It was manufactured from 7075-T6 Aluminum alloy, with design pressure ratio 1.8 and 80% efficiency. The rotor was experimentally measured to have 1.69 pressure ratio and 72% efficiency. It was recently run to a pressure ratio of 2.0 with an increase in efficiency by 0.36% at 100% speed and 0.29% at 90% speed at a variant clearance [14], [15].

An Automated mechanical optimization system has been developed for the transonic fan minimizing the blades mass followed by an aerodynamic optimization to maximize the efficiency and/or stall margin as objective function(s). A parametric definition of the geometry allows a wide range of designs. Fig. 5 shows the NPS transonic fan rotor design.

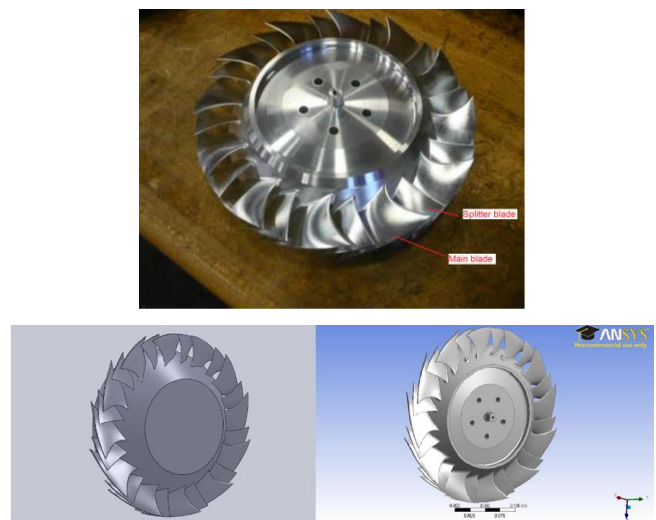


Fig. 5. NPS designed transonic fan rotor [11].

V. CALCULATION OF THE INITIAL DESIGN PARAMETERS

The pressure ratio (PR) and adiabatic efficiency (η_{ad}) are the design targets as mentioned in the NPS design report [11] such that,

$$PR = 2, \eta_{ad} = 0.8 \quad (3)$$

From NPS experimental measurements for the manufactured transonic fan, the specific inlet mass flow rate is measured to be 171.3 kg/s/m^2 . By using the rotor inlet area (A_{in}), mass flow rate (\dot{m}) is calculated to be,

$$\begin{aligned} \dot{m} &= \dot{m}_s A_{in} \\ \dot{m} &= 6.0548 \text{ kg/s} \end{aligned} \quad (4)$$

Deriving an equation to estimate the inlet Mach number,

$$\begin{aligned} \dot{m} &= \rho v A_{in} \\ \dot{m} &= \rho (M \sqrt{\gamma RT}) A_{in} \\ M &= \frac{\dot{m}}{\rho A_{in} \sqrt{\gamma RT}} \end{aligned} \quad (5)$$

where, ρ is the inlet air density, v is the inlet air velocity, M is the inlet Mach number and T is the stagnation temperature.

Equation (5) along with the stagnation pressure and temperature ratio together with the equation of state, a nonlinear Mach number equation is obtained,

$$\begin{aligned} M &= \frac{\dot{m}}{\frac{P}{RT} A_{in} \sqrt{\gamma RT}} \\ M &= \frac{\dot{m}}{A_{in} \sqrt{\gamma}} \sqrt{\frac{R}{P} \frac{T}{P_o} \frac{T_o}{P_o}} \\ M &= \frac{\dot{m}}{A_{in} P_o} \sqrt{\frac{RT_o}{\gamma}} \left(1 + \frac{\gamma-1}{2} M^2 \right)^{\left(\frac{\gamma}{\gamma-1} \frac{1}{2} \right)} \end{aligned} \quad (6)$$

Solving this nonlinear Mach number equation (6), the inlet Mach number for this transonic fan is,

$$M_{in} = 0.4669$$

VI. T-AXI AND 3DBGB DESIGN

T-AXI [12] has been used to create the transonic fan design input files for 3DBGB. TCdes (Turbomachinery Compressor Design) [12] is a part of the T-AXI suite of codes. It is used to create the initial input files using the initial calculated design parameters (walls and stack files). The rotor design point rotational speed is 27000 RPM (as in the NPS report).

The 3DBGB input files for the main and splitter blades include the streamlines, blade leading and trailing edges splines which are plotted in Fig. 6 and Fig. 7.

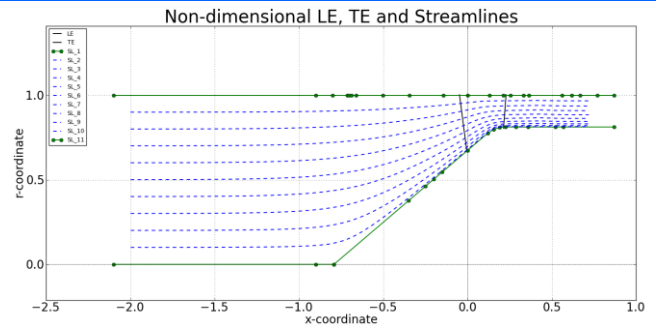


Fig. 6. Non-dimensional main blade input streamlines plot with leading and trailing edges splines.

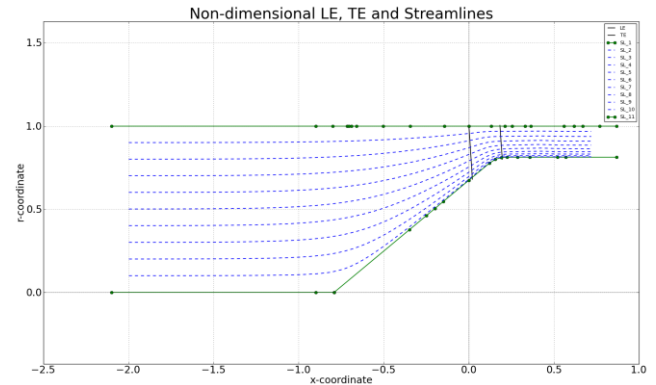


Fig. 7. Non-dimensional splitter blade input streamlines plot with leading and trailing edges splines.

The inlet and exit metal angles for the main and splitter blades are also plotted as a check for the spanwise smooth transition between blade section inlet and exit angles as shown in Fig. 8 and Fig. 9.

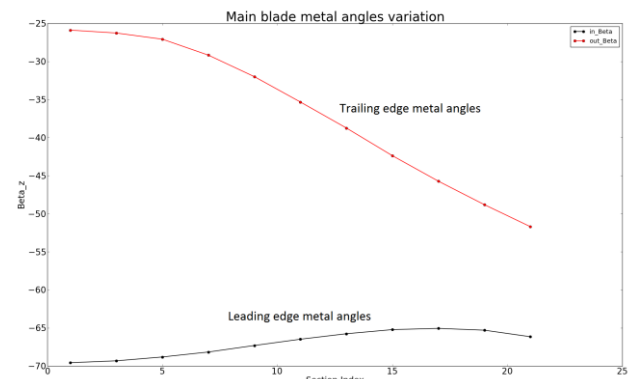


Fig. 8. Transonic fan main blade metal angles.

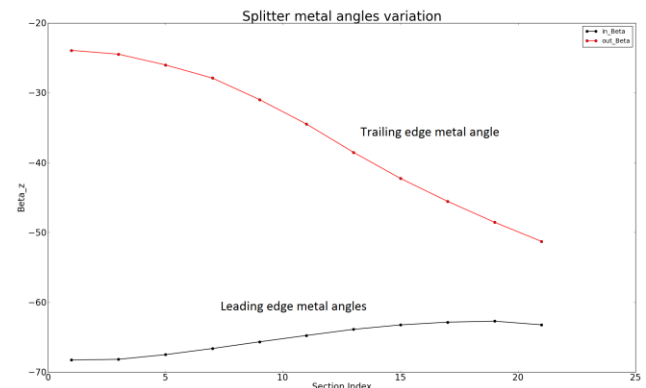


Fig. 9. Transonic fan splitter blade metal angles.

The outputs from the 3DBGB design program are 2D and 3D sections for the main and splitter blades. The $(m' - \theta)$ 2D airfoils are plotted as shown in Fig. 10 and Fig. 11.

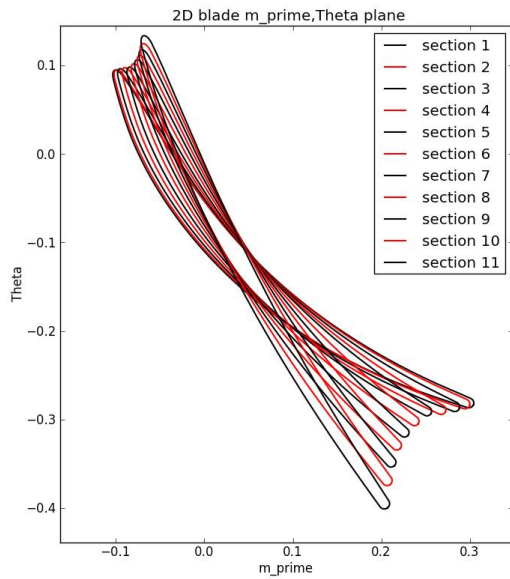


Fig. 10. The $(m' - \theta)$ main blade 2D airfoils.

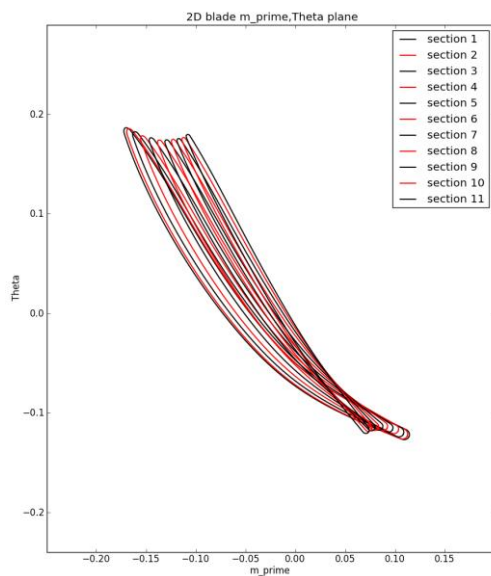


Fig. 11. The $(m' - \theta)$ splitter blade 2D airfoils.

The outputs from 3DBGB design process are used in the next optimization step.

VII. STRUCTURAL OPTIMIZATION:

A. Baseline

Through the optimization process, maximum stress is assigned to be a constraint (safe percentage of the max. yield strength of the material). The SolidWorks (SW) model creation is automated for the optimization purpose. A MATLAB code, originally created in Naval Postgraduate School [11], [15] to draw the blade flow path, has been modified to create and name the rotor blades sector. The MATLAB code is connected to SolidWorks to create the imported geometry from 3DBGB output files. The static structural analysis (ANSYS) uses a MATLAB script to refresh the analysis

with the newly created geometries through the optimization process.

The rotor disk sector is created using the periodic pitch angle $(\theta_{pitch} = \frac{2\pi}{N_{blades}})$ where, N_{blades} is the number of the blades in the rotor. The SW rotor sector is created using the 3DBGB description of the blade as shown in Fig. 12.

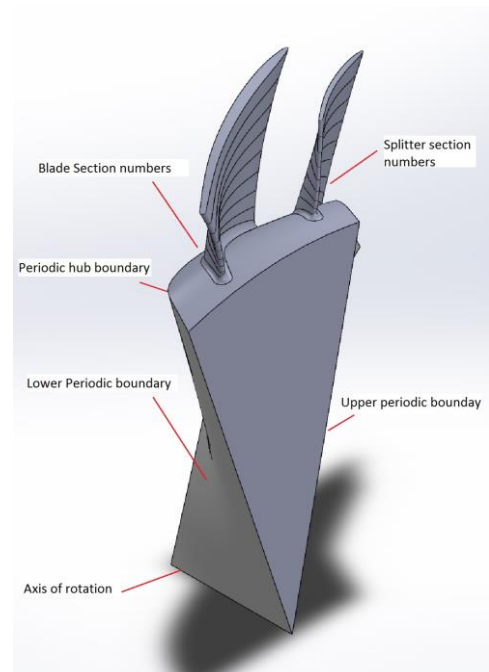


Fig. 12. Transonic fan rotor sector created on SolidWork using MATLAB script

The static structural analysis problem is performed by defining a cylindrical coordinate system, boundary conditions, centrifugal load, and design constraints. The material used by Scott [11] was the 7075-T6 Aluminum alloy for the blisk fan with properties listed in TABLE I. ,

TABLE I. ALUMINUM ALLOY PROPERTIES.

7075-T6 Aluminum alloy	
density	2804 kg/m ³
Tensile yield strength	503 MPa
Ultimate Tensile Strength	572 MPa
Modulus of Elasticity	71.7 GPa

Symmetric cyclic boundary conditions are assigned to the disk sector. When the solid model is imported to ANSYS static structural module, the "Named selections" features are imported with their assigned names. This allows automatic update with the new geometry even if the features were changed.

B. Grid resolution study for Mechanical Analysis

A grid resolution study for static structural module is performed for the initial design to decide the grid level to use in the optimization process.

Four grid levels were chosen for the comparison. The grid sizing is based on curvature size function (setting curvature normal angle to 45°) with medium smoothing and fast grids transition for the first three grid (coarse, medium, fine). The fourth grid is the very fine grid, the grid sizing is chosen based on curvature and proximity with curvature normal angle of 40°. The smoothing for the last grid is taken “high” with slow transition between grid levels.

Centrifugal load is applied to the model with designed rotational speed of 27000 rpm. The case constraints are defined and the model is solved with direct matrix solution (for more accurate results).

The results from the different grid levels are compared in TABLE II. The number of each level grid nodes indicates its calculation time. The medium grid level has almost half the number of nodes of the fine grid and about 1/8 nodes of the very fine grid. The change in deflections between medium, fine and very fine grids are relatively small. Although, there are differences in maximum stress values, the medium grid level is adequate to use for this fidelity of optimization. As for the final optimum design, the accuracy needs to increase using a finer grid.

TABLE II. COMPARISON BETWEEN DIFFERENT GRID LEVELS.

Grid level	Coarse	Medium	Fine	Very Fine
Number of Nodes	41955	58197	126840	1000826
Number of cells	23928	34336	79943	677260
Total Deformation [mm]	0.4556	0.4587	0.4603	0.463
Radial Deformation [mm]	0.1928	0.1933	0.19356	0.1941
Tangential Deformation [mm]	0.2344	0.2362	0.23707	0.2385
Axial Deformation [mm]	0.1121	0.1154	0.1171	0.1182
Maximum stress [GPa]	0.3801	0.3834	0.386	0.3872

VIII. CFD OPTIMIZATION :

A. Baseline

Two CFD baseline cases were created as a starting point for CFD optimization. The first baseline is at the design point (100% full speed) while the other is at a part speed (60% full speed). The geometry used for both cases are the mechanically optimized design that have lower mass and meet the stress constraints. The geometry is defined using previously created “geomturbo” script [12], [13] after being modified to support splintered rotors. The grid is created such that it supports 3 multigrid levels. A CFD test case for the transonic fan is created to evaluate rotor efficiency (η) at 100% full speed and static pressure recovery factor (C_p) at part speed (60% full speed). Tip clearance is set to 0.51 mm for both main and splitter blades. The main blade hub fillet is 2.145 mm and the splitter fillet is 2.165 mm. The design conditions for the design and part speeds test cases are shown in TABLE III.

TABLE III. DESIGN CHART FOR THE TRANSONIC FAN AT DESIGN SPEED.

Design parameter	Value
Tip Diameter [m]	0.1435
Main blade aspect ratio	0.528
Splitter blade aspect ratio	0.804
Tip speed [m/s]	405.79
RPM	27000
Design Mass flow [kg/s]	4.94
Design Total Pressure ratio	1.759

The boundary conditions for the test case are stated in TABLE IV.

TABLE IV. BOUNDARY CONDITIONS FOR THE TRANSONIC FAN TEST CASE.

Conditions	Value
Inlet Total Pressure	101335 [Pa]
Inlet Total Temperature	288.15 [K]
Design point speed (100% full speed)	27000 [RPM]
Part speed (60 % full speed)	16200 [RPM]
Design point static back pressure at radius 0.117 m (Radial equilibrium)	130000 [Pa]
Part speed static back pressure at radius 0.117 m (Radial equilibrium)	100000 [Pa]

The results from these cases are considered as the baseline starting points for the CFD optimization. The model used is the Spalart Allmaras (Extended wall function). Fig. 13 and Fig. 14 show the meridional flow path and blade to blade meshing at 50% span.

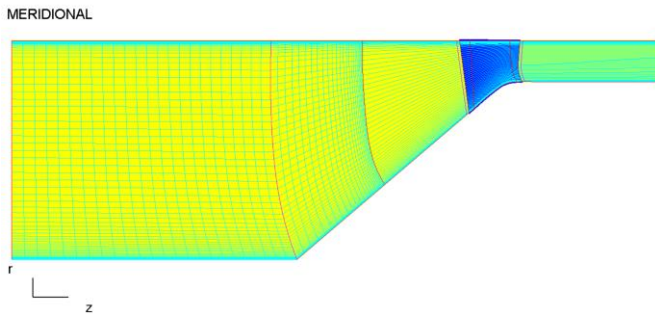


Fig. 13. The ($m' - \theta$) splitter blade 2D airfoils.

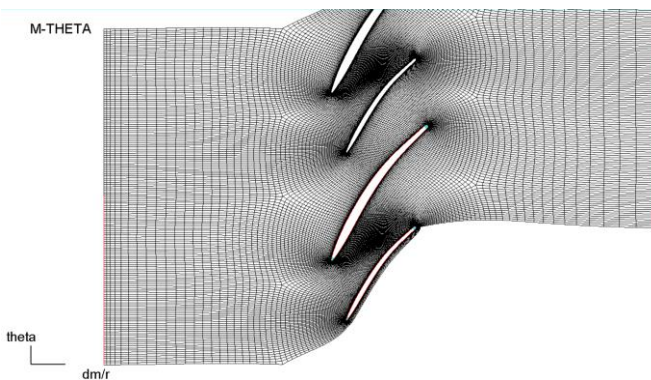


Fig. 14. Blade to blade mesh at 50% span.

B. Grid Dependency study for CFD Analysis

To choose which grid to use and how the optimization objective functions depend on the grid level, a grid dependency study is performed. Three levels of grid exist in Fine/Turbo, “222”, “111” and “000” graded from course to fine grid quality respectively. The fine grid, “000”, is set up in the grid generator Autogrid, and the “111” grid has $\frac{1}{2}$ the grid cells in each direction, and therefore $\frac{1}{2}$ the number of grid points. The “222” grid is half the “111” grid in 3 directions so $\frac{1}{8}$ the total grid points. The mass flow rate, efficiency and pressure ratio are the outputs that specify the design performance. Three test cases were established using the three levels of grids for the design point. The number of grid points is shown in TABLE V.

TABLE V. NUMBER OF GRID POINTS FOR EACH GRID LEVEL.

Grid Level	Number of Grid points
“222”	52,360
“111”	364,194
“000”	2,706,658

The spatial discretization scheme used for the three grid levels was the second order upwind scheme. A

central scheme was used to start the “222” coarse grid levels, and then the second order upwind scheme is used. The “111” grid level case is initialized from the “222” grid level solution using the second order upwind scheme. Similarly, “000” initiated with “111” grid level solution and used the second order upwind scheme. The inlet and outlet mass flows, pressure ratio and efficiency were compared for the three levels of the grids as shown in TABLE VI. .

TABLE VI. COMPARING OUTPUTS FROM EACH GRID LEVEL.

Grid Level	inlet mass flow	outlet mass flow	Efficiency	Pressure Ratio	Temp. Ratio
“222”	4.8807	4.888	0.7755	1.7778	1.2307
“111”	4.9469	4.949	0.7873	1.7595	1.2225
“000”	4.9421	4.943	0.7872	1.7563	1.2218

Results show an acceptable matching between the “111” and “000” grids. The mass flow rate varies from 0.097% to 0.135% while the efficiency and pressure ratio varies by 0.024% and 0.182% respectively. For an optimization consideration, the “111” grid level will give acceptable results considering difference in grid size between the fine and medium grids.

IX. RESULTS

The automated structural and CFD optimization loops are performed with different optimization techniques. The mechanical loop starts with the initial 3DBGB design for both the main blade and splitter. Then using the 3D sections, the MATLAB code creates the SW solid model as a periodic sector. The mechanical optimization loop is set up to reduce the rotor mass while constraining the maximum stress. The CFD optimization process uses the mechanically optimized design as a starting point. A “geomturbo” file is created to be used by AUTOGRID (NUMECA) [10] for gridding. The CFD optimization is set up to maximize the efficiency and/or stall margin with/without constraining the mass flow rate and pressure ratio. Test cases are run to explore different optimization strategies.

A. Structural Optimization Results

The fan initial design stress distribution is shown in Fig. 15. A minimization of the blade mass is desired while constraining the maximum Von-Mises stress below 50% of the material yield strength ($\sigma_{von-mises} \leq 0.5\sigma_{yield-Al-7075}$). This optimization is performed to ensure a safe design from the structural point of view before doing the time consuming fluid dynamics optimization.

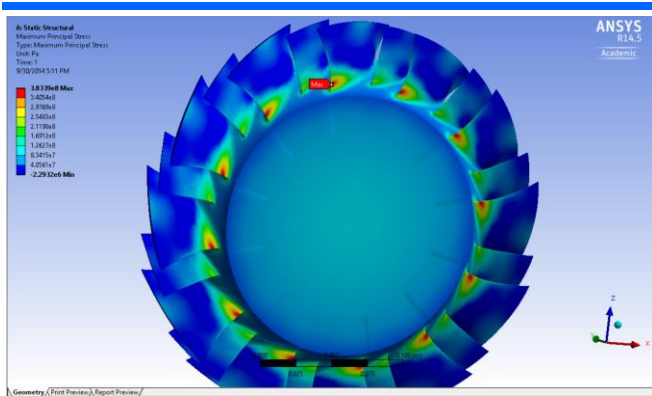


Fig. 15. Stress distribution of the fan initial design.

The structural optimization process is performed by varying two effective geometry parameters which are:

1. The span-wise spline of maximum thickness multiplier (t_m/c): This variable multiplies the predefined blade thickness distribution by a spline factor that has its control points defined in the 3DBGB input file. The default value for the spline maximum thickness multiplier is 1.0. Fig. 16. demonstrates the spline thickness multiplier on the 3rd section of the main transonic fan blade in ($m' - \theta$) space with a factor of 1.3

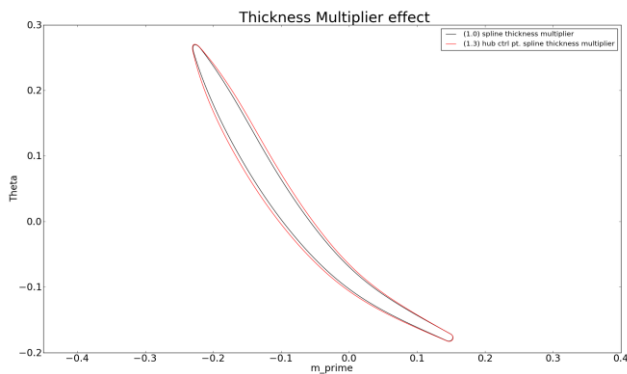


Fig. 16. Span-wise spline thickness multiplier effect for the 3rd section in ($m' - \theta$) space.

2. The second parameter is the spline chord multiplier ($chrd_{multi}$). This is a spline defined multiplier for predefined chord distribution. The spline chord multiplier effect with factor of 1.14 is shown in Fig. 17 in the ($m' - \theta$) space. The default value for the spline chord multiplier is 1.0

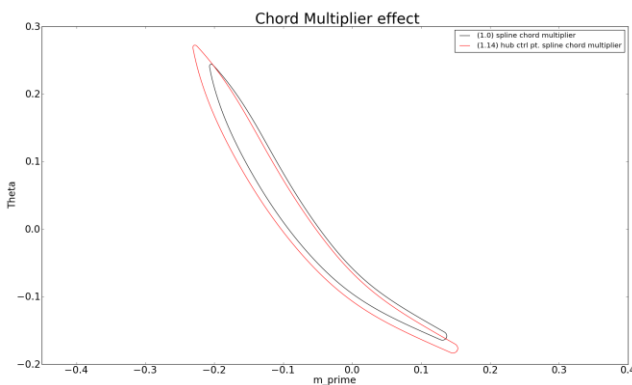


Fig. 17. Span-wise chord multiplier effect for the 3rd section in ($m' - \theta$) space.

These two geometric parameters were chosen to reduce stress concentration below constraints. The concentration of maximum stress is observed to be at the hub sections as shown in Fig. 15. The spline chord multiplier is chosen to change the 35% span-wise from the hub section. The actual effect of the two variables is studied through the parametric study.

1) Parametric study:

A parametric study using the mechanical optimization loop is performed to find out the effect of each parameter on optimization process.

One parametric study was done for the spline chord multiplier for both the main and splitter blades. As the hub chord increases, the angle between the blade surface and the hub surface increases. This increase in the angle reduces the fillet radius that is created in the SW 3D model generation as shown in Fig. 18.

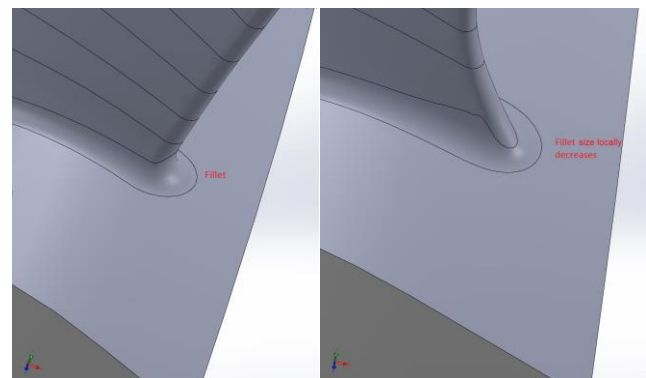


Fig. 18. Initial design fillet size & Fillet radius decreases with chord increase

This 3D effect allows the blades mass to decrease with increasing chord multiplier at the first three evaluations while the maximum stress still decreases. At higher chord length the fillet radius is not decreasing much so the mass of the blades increases as the chord increases. The stress at larger chords starts to increase because the thickness ratio is still constant while chord length increases. This explains why both t_m/c and $chrd_{multi}$ should be used simultaneously to reduce stress concentrations on the blades root sections.

2) Hybrid optimization strategy:

A Genetic Algorithm optimization is created starting with the initial geometric design point to find a global minimum for the objective function. A numerical gradient optimization is done starting with the genetic algorithm results to find any other optimized design if one exists.

A single objective genetic algorithm method (SOGA) is used for minimizing the blade mass and constraining the maximum Von-Mises stress.

The ranges for the optimization variables are chosen according to the parametric study. The span-wise spline thickness multiplier range is [1.0, 1.5] and the span-wise spline chord multiplier range is [1.0, 1.2].

The variations of the optimization parameters with objective function and constraint output are plotted in Fig. 19. The plot shows the effect of the thickness multiplier on the change in blades mass that indicates the parameter effectiveness. The two parameters together are affecting the rotor maximum stress.

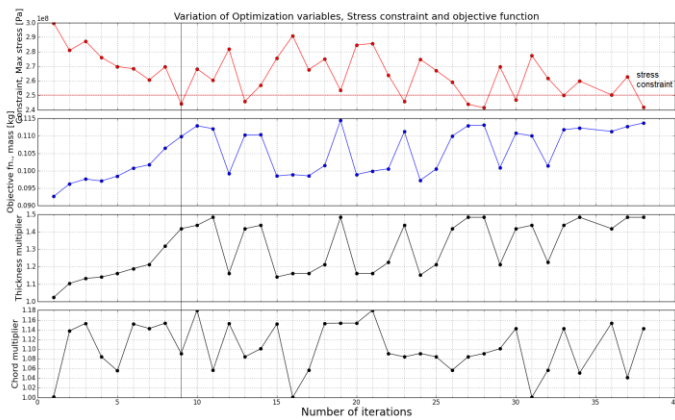


Fig. 19. Geometric variables variation with objective function and constraint for SOGA optimization.

The best evaluation was found to be the 9th evaluation. The results are compared with the baseline case in TABLE VII. . A redistribution of the blade sections chords and thicknesses decreases the maximum stress while keeping the blades mass nearly the same.

TABLE VII. BASELINE AND OPTIMIZED OBJECTIVE FUNCTION AND CONSTRAINT FOR GA OPTIMIZATION.

Property	Baseline values	Optimized Values
Blade mass [kg]	0.10825	0.10983
Max. Von-Mises stress [MPa]	383.39	244.049
Main blade thickness multiplier	1.0	1.4179
Main and splitter blades chord multiplier	1.0	1.09072

The output from GA was used as a starting point for a gradient based optimization to refine the GA optimum design in a smaller range. TABLE VIII. shows the starting point and the refined design. The refinement allows the decrease of the blades mass with a little increase in the maximum stress. The maximum stress is still below the upper bound (50% yield strength of the material).

The maximum stress has dropped below the constraint as seen in the ANSYS stress contour in Fig. 20. This represents a structurally hybrid optimization design to start the CFD optimization process.

TABLE VIII. GENETIC ALGORITHM OPTIMIZED DESIGN AND RESULTING GRADIENT REFINED OPTIMIZATION COMPARISON.

Property	Baseline values	Optimized Values
Blade mass [kg]	0.109828	0.105428
Max. Von-Mises stress [MPa]	244.04941	249.55925
Main blade thickness multiplier	1.417881	1.300308
Main and splitter blades chord multiplier	1.090719	1.141799

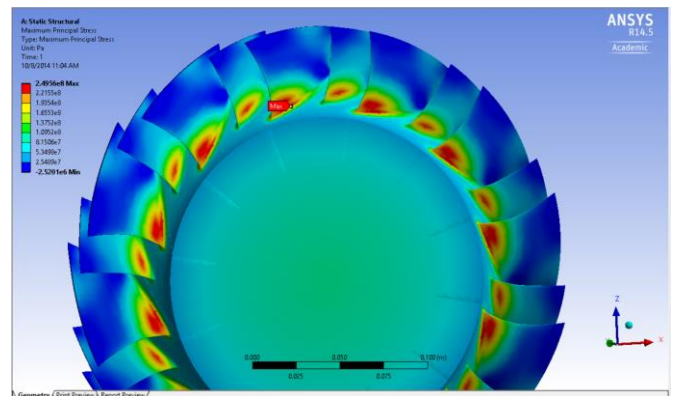


Fig. 20. Stress distribution for the optimized geometry.

B. CFD Optimization Results:

1) Speed line for mechanical optimization baseline design at full speed (100%):

A CFD analysis is performed on the mechanically optimized blades. The operating speed is 100 % full speed (27000 rpm). An exit static pressure was found such that, the inlet mass flow didn't increase even with a decreased back pressure. The speed line is created starting from choked exit pressure then increasing the exit static pressure until reaching stall point.

The speed line was calculated and plotted as shown in Fig. 21 and the rotor design point is specified.

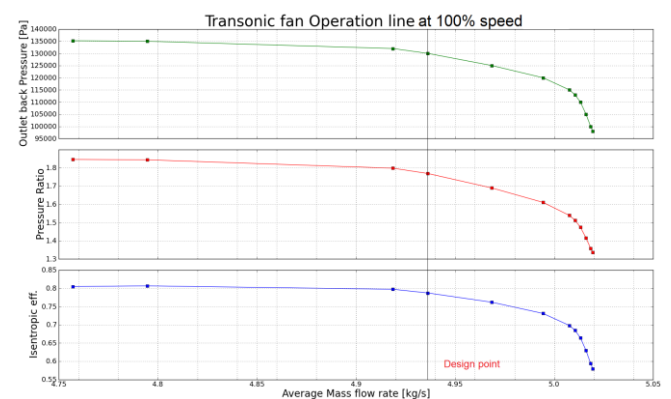


Fig. 21. The Transonic fan speed line at 100% full speed.

2) Speed line calculation for the Mechanically optimized rotor at part speed (60%):

The calculation of pressure recovery factor is done at a part speed of 60% full speed. The speed line for the mechanically optimized transonic fan design is calculated and plotted as shown in Fig. 22,

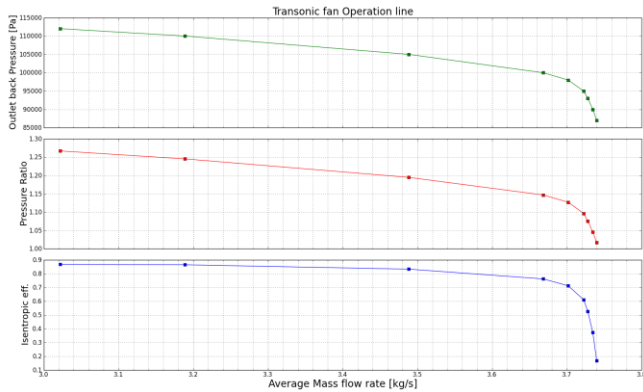


Fig. 22. The Transonic fan speed line at 60% full speed (part speed).

The speed lines for the part and full speeds are plotted together with the operating line (throttle line) to obtain the part speed design point as shown in Fig. 23,

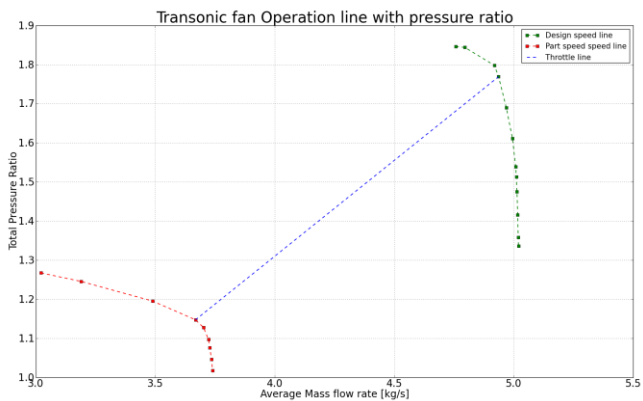


Fig. 23. The design point and part speed intersection with the throttle line.

The static pressure recovery factor is also plotted with the mass flow rate as shown in Fig. 24 that indicates lower C_p while increasing the mass flow rate (working at 60% full speed improves the stall margin)

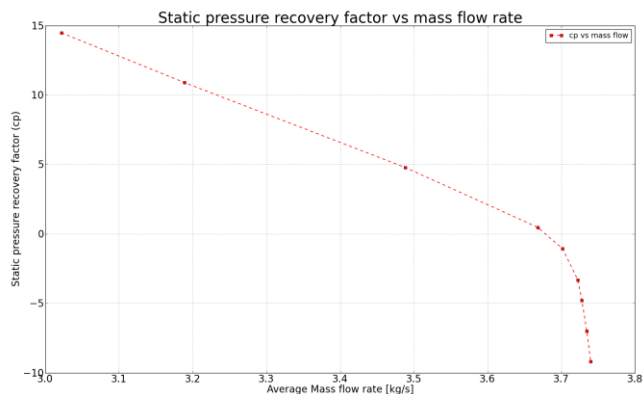


Fig. 24. Static pressure recovery factor change with mass flow rate.

The static pressure recovery factor is calculated at the intersection point of throttle line and 60% speed line for a back static pressure 100000 [Pa] as follows,

$$C_p = \frac{P_2 - P_1}{P_{01-rel} - P_1}$$

$$C_p = \frac{100498.56 - 99998.68}{101335.00 - 99998.68}$$

$$C_p = 0.374072 \quad (6)$$

This is evaluated using the 60% full speed during the C_p optimization process. This should improve the off design operating range besides improving the design point efficiency at 100% full speed.

The "111" grid level template files are created at the full and part speeds for the CFD optimization problem. A Python script is created to run the CFD to run in the batch mode. The CFD calculations were done in parallel processing mode tailored for the available computing resources.

3) Single objective Genetic Algorithm (SOGA) CFD optimization for efficiency " η ":

An unconstrained SOGA optimization is done to minimize " $1 - \eta$ " (Maximize efficiency " η "). The structurally hybrid optimized geometry is used as a baseline for the optimization and efficiency is calculated at 100% speed (27000 RPM). The two middle control points of the second derivative of the camber line B-spline (resemble the camber curvature) are the optimization parameters. The curvature is changed for the main and splitter blades span-wise. The SOGA configuration is kept the same as the structure optimization problem. The optimization is unconstrained to check for system reliability of the tandem design space.

A plot of " $1 - \eta$ " minimization is shown in Fig. 25. The mass flow rate and pressure ratio are tracked through the optimization process to allow using them as constraints in the next optimization runs. The evaluation number "52" is the best evaluation.

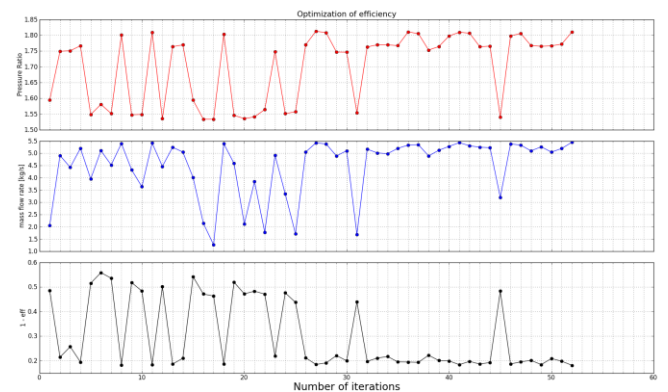


Fig. 25. DAKOTA efficiency optimization.

The baseline and efficiency optimized curvatures are compared in Fig. 26 and Fig. 27. In Fig. 27, the curvature of the splitter changes sign twice yields on "S-shaped" blade.

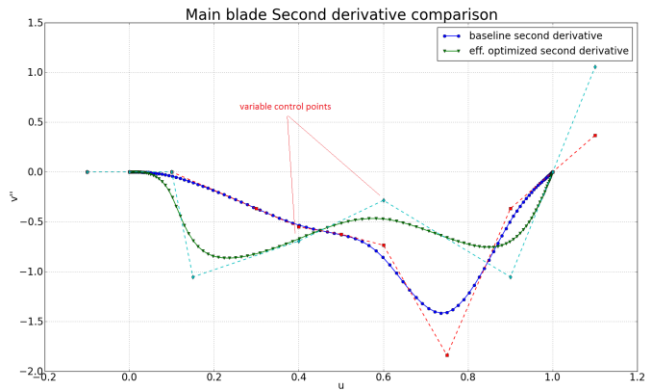


Fig. 26. The main blade baseline and eff. optimized curvatures.

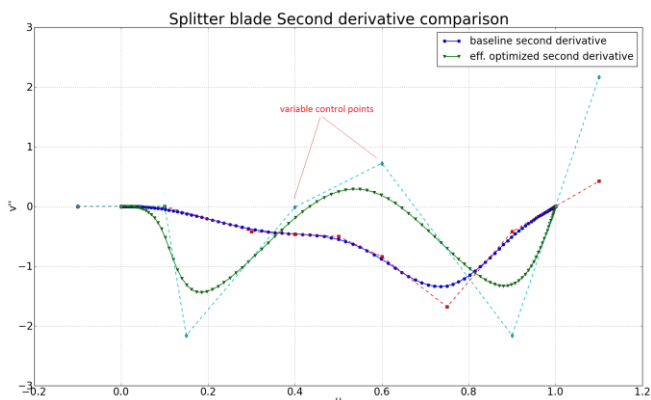


Fig. 27. The splitter blade baseline and eff. optimized curvatures.

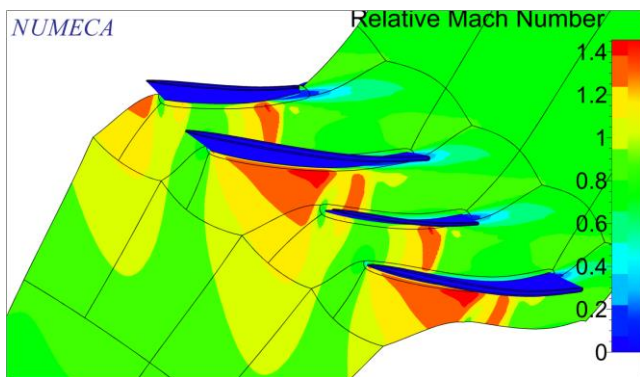


Fig. 28. Relative Mach number for baseline design.

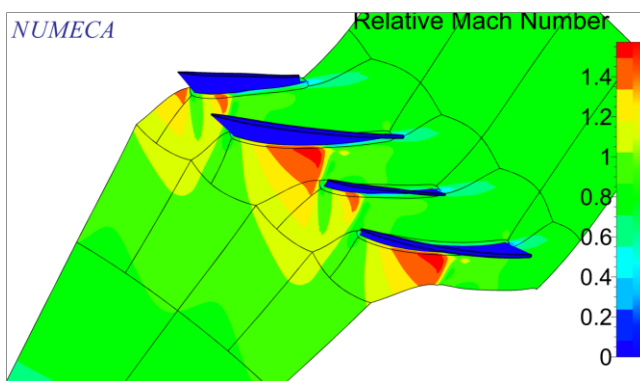


Fig. 29. Relative Mach number for efficiency optimized and efficiency designs.

Fig. 28 and Fig. 29 shows the difference between the baseline and efficiency optimized relative Mach number at 50% span. The change in blade curvature weakens the flow passage normal shock waves which reduces the losses and consequently increases the efficiency.

A comparison between the baseline design and efficiency optimized parameters are shown in TABLE IX.

TABLE IX. EFFICIENCY OPTIMIZATION RESULTS.

Property	hybrid mech. optimized	Efficiency Optimized
Isentropic Efficiency	0.784	0.819
Mass flow [kg/s]	4.944	5.448
Total Pressure ratio	1.759	1.811

4) Single objective Genetic Algorithm (SOGA) CFD optimization for static pressure recovery factor (C_p):

An unconstrained SOGA optimization is done to maximize the static pressure recovery factor (C_p) by minimizing $-C_p$. The static pressure recovery factor is evaluated at part speed (60 % full speed = 16200 RPM).

Minimization of $-C_p$, while keeping track of the mass flow rate, pressure ratio and efficiency are shown in Fig. 30. The "27" evaluation is chosen by the optimizer as the best evaluation.

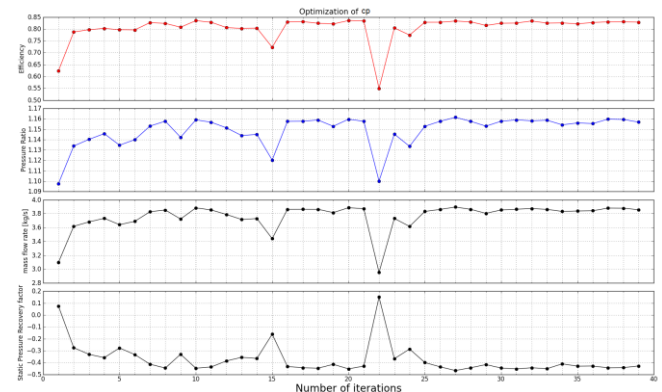


Fig. 30. DAKOTA Stall Margin Optimization.

The optimized main and splitter blades curvatures are in Fig. 31 and Fig. 32.

A comparison between the hybrid mechanically optimized and C_p optimized parameters are shown in TABLE X.

Fig. 33 and Fig. 34 shows a comparison between the hybrid mech. optimized and stall margin optimized relative Mach number at 50% span. The change in the curvature results in suppressing the relative flow speed to the subsonic level. This increases the fan stall margin in the off-design conditions.

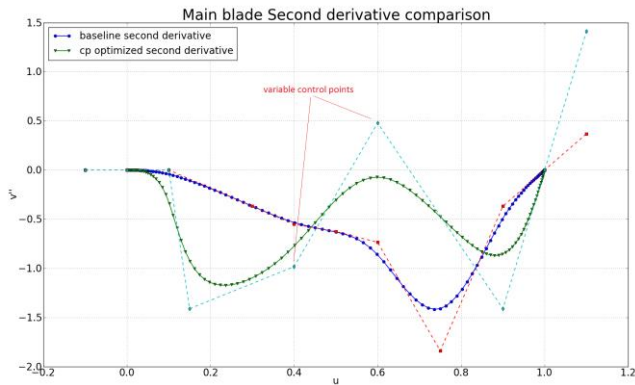


Fig. 31. The main blade hybrid mechanically optimized and C_p optimized design curvatures.

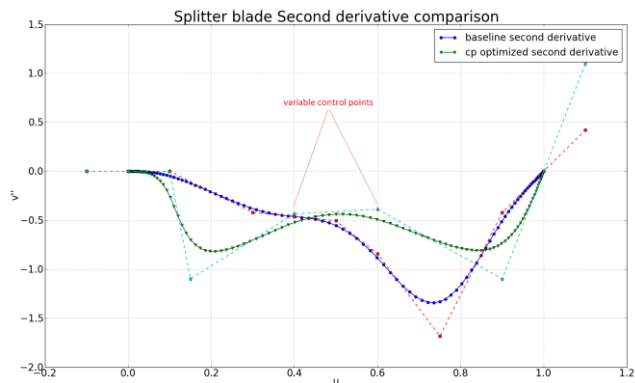


Fig. 32. The splitter blade hybrid mechanically optimized and C_p optimized design curvatures.

TABLE X. STALL MARGIN OPTIMIZATION RESULTS.

Property	hybrid mech. optimized	C_p Optimized
Static Pressure Recovery	0.374072	0.4668215
Isentropic Efficiency	0.78364	0.83296
Mass flow [kg/s]	3.6715	3.8961
Total Pressure ratio	1.1456	1.1614

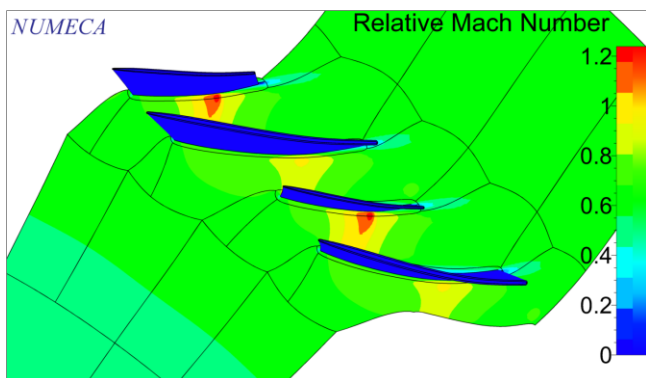


Fig. 33. Hybrid mech. optimized relative Mach number.

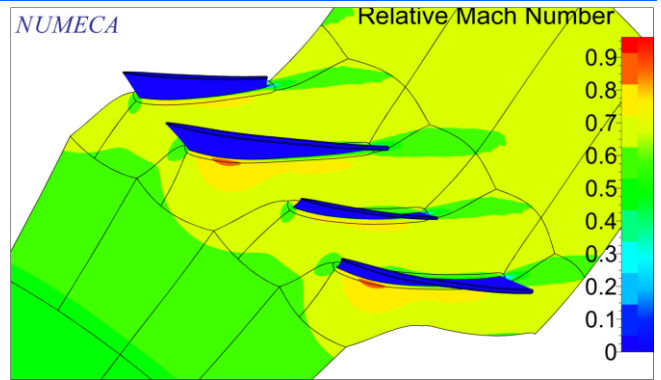


Fig. 34. Stall margin optimized relative Mach number.

5) Multi Objective Genetic Algorithm (MOGA) CFD optimization for both " η " and " C_p ":

A constrained multi objective function optimization using Genetic Algorithm (MOGA) is created. " $1 - \eta$ " and " $-C_p$ " objective functions are minimized in a trade-off. The mass flow and pressure ratio are constrained in the following ranges,

$$2 \leq \dot{m} \leq 7$$

$$1.2 \leq PR \leq 2.5$$

A Pareto is plotted between efficiency and stall margin as shown in Fig. 35.

Pareto plot between efficiency and stall margin

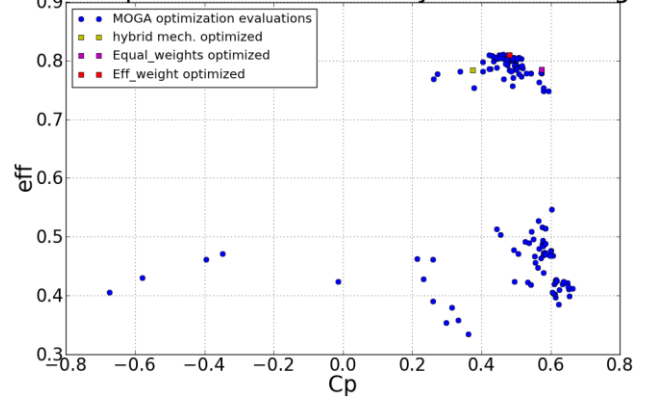


Fig. 35. Pareto plot between efficiency and static pressure recovery factor.

Pareto Front between efficiency and stall margin

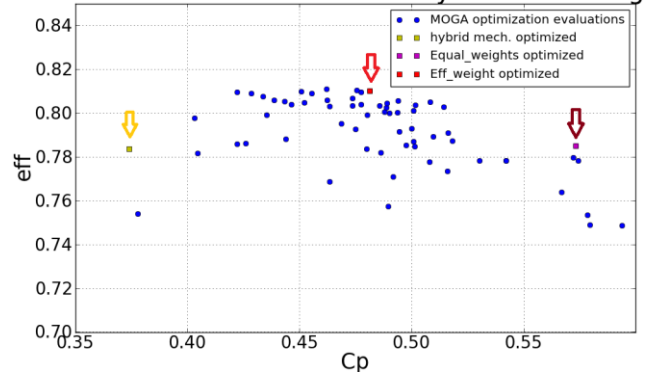


Fig. 36. Pareto front between efficiency and static pressure recovery factor.

The Pareto front is plotted in Fig. 36 showing two optimum points for this case. The first has an equally

weighted tradeoff between efficiency and stall margin (equal_weights). The second point has more weight for efficiency than stall margin (eff_weight). The later allows a higher efficiency design point with a narrow stall margin.

The baseline and the two optimization points are compared in the TABLE XI. The trade-off between the efficiency and stall margin will depend on the purpose of the design. For commercial engines, a higher efficiency will be much important than a wide stall margin although for military ones, the stall margin will be an important recommendation for the off-design maneuvers.

TABLE XI. EFF. AND CP OPTIMIZATION RESULTS.

Property	hybrid mech. optimized	eff and cp Optimized (Eff_weight)	eff and cp Optimized (equal_weights)
Static Pressure Recovery at part speed	0.374	0.48123	0.573
Isentropic Efficiency at design point	0.784	0.8102	0.785
Mass flow at design point [kg/s]	4.944	5.388	5.041
Total Pressure ratio at design point	1.759	1.818	1.8301

The baseline and eff_weight optimized curvatures for the third sections from root are compared for the main and splitter blades in Fig. 37 and Fig. 38. The blade and splitter curvature profiles look very similar with a constant curvature at the mid chord. This curvature profile was similar to the transonic EEE curvature that was discussed in a previous article [9].

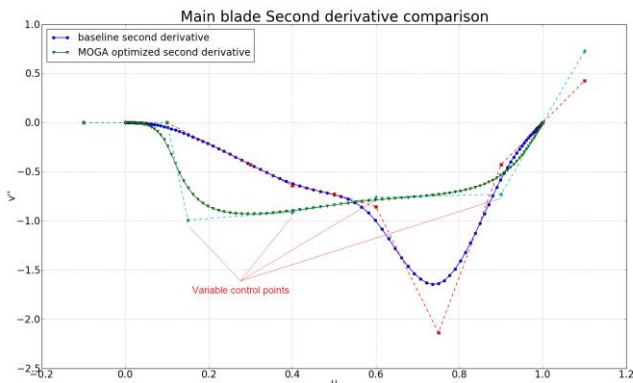


Fig. 37. The main blade hybrid mech. optimized and eff_weight optimized curvatures.

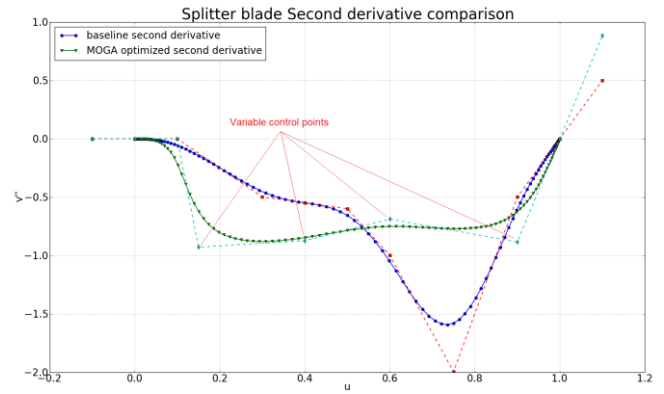


Fig. 38. The splitter blade hybrid mech. optimized and eff_weight optimized curvatures.

Fig. 39 shows eff_weight optimized relative Mach number at 50% span. The flow passage normal shocks are suppressed relative to the baseline design with the higher blades curvature.

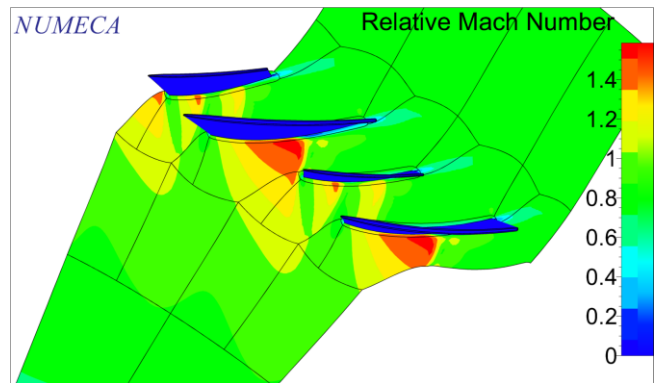


Fig. 39. Efficiency and weight (eff_weight) optimized relative Mach number contours.

C. Timing Report

Another important aspect that should be mentioned is the timing report. The timing for the structural and 3D CFD multi-objective optimization are listed in TABLE XII. and TABLE XIII.

TABLE XII. STRUCTURAL OPTIMIZATION TIMING REPORT. THE 3DBG, DEFLECTION PROCESSING SCRIPT AND TIP PROFILE CREATOR HAVE TIME IN THE ORDER OF SECONDS.

Process	Avr. time [min]	Number of cores	Core speed [GHz]	Successful runs	Failed runs	Total time [min]
SolidWorks 3D model	0.5	1	2.6	37	3	18.5
ANSYS stress analysis	9.0	1	2.6	37	3	333
Total computing time for Structural optimization						5.85 [hrs]

TABLE XIII. CFD OPTIMIZATION TIMING REPORT. THE 3DBGB, GEOMTURBO, DEFLECTION PROCESSING SCRIPT AND TIP PROFILE CREATOR HAVE TIME IN THE ORDER OF SECONDS.

Process	Avr. time [min]	No. of cores	Core speed [GHz]	Success runs	Failed runs	Total time [min]
AUTOGRID grid generator	8.2442	1	2.2	135	15	1112.96
FINE/TURBO flow solver (η)	18.130	9	2.2	135	15	2447.56
FINE/TURBO flow solver (C_p)	17.714	9	2.2	135	15	2370.76
Total computing time for MOGA optimization						98.86 [hrs]

The optimization loop scripts discard the bad geometries and assign them as failed runs. The processing time do not include the failed runs. The flow solver was done with parallel processing. Each MOGA evaluation is done with two evaluations, one at full speed and the other at part speeds.

X. CONCLUSIONS:

A multidisciplinary design optimization system has been created and applied to a splintered transonic fan as a test case. The geometry definition uses an open executable code developed at the University of Cincinnati [7].

Using the parametrically designed blades, the system is set to constrain the mechanical loading of the design. The maximum rotor stress is checked and compared with 50% (safety factor chosen) of the maximum material yield strength. The structural optimization system creates a mechanically accepted design at an optimized mass. A CFD optimization system has been created to optimize the efficiency and/or the stall margin.

Several runs have been performed to demonstrate the optimization process:

1. Single objective Genetic Algorithm (SOGA) mechanical optimization followed by a numerical gradient optimization is done to minimize the blades mass while constraining the maximum stress on the rotor. A span-wise spline thickness and chord multipliers are used as variables throughout the optimization process to reduce the stress concentrations.

2. An unconstrained SOGA CFD optimization is performed on the mechanically optimized design. The objective was to maximize the efficiency and/or pressure recovery factor. The control points of the second derivative spline (curvature) defining the blade sections camber-line are used as the optimization variables. The mass flow rate, pressure ratio, efficiency and static pressure recovery factor are all

monitored through several optimizations to decide the desired design point for the constrained optimization.

3. Multi objective Genetic Algorithm (MOGA) CFD optimization is performed on the mechanically optimized transonic fan. This was a trade-off between the efficiency and stall margin. For “eff_weight” design, optimizing the curvature of the main and splitter blades section camber-lines increases the efficiency by 2.651% and the off design pressure recovery by 28.64%.

Having the designer in the optimization loop is important to drive towards the desired optimized design. Eliminating the designer role is not recommended such that efficient parameters and acceptable designs are chosen while optimization time is reduced.

ACKNOWLEDGMENTS

I gratefully acknowledge the support and generosity of the Egyptian Army for funding my PhD research. Thanks for Jake Holden for helping with the FINE/TURBO batch mode commands. Thanks to Sam Somtrakool for his help to create Static Structural commands for automatic extraction of deformations.

REFERENCES

- [1] E. Benini, “Three-Dimensional Multi-Objective Design Optimization of a Transonic Compressor Rotor,” *Journal of Propulsion and Power*, Vol. 20, No. 3, May - June 2004, pp. 559 – 565.
- [2] C.-M. JANG, P. LI, and K.-Y. KIM, “Optimization of Blade Sweep in a transonic Axial Compressor Rotor,” *JSME International Journal*, Vol. 48, No. 4, 2005, pp. 793 – 801.
- [3] Y. Lian and M.-S. Liou, “Multi-Objective Optimization of Transonic Compressor Blade Using Evolutionary Algorithm,” *JOURNAL OF PROPULSION AND POWER*, Vol. Vol. 21, No. 6, 2005, pp. 979 – 987.
- [4] L. Ellbrant, L.-E. Eriksson, and H. Martensson, “Design of Compressor Blades considering Efficiency and Stability using CFD based Optimization,” *GT2012-69272 ASME Turbo Expo*, 2012.
- [5] L. Ellbrant, L.-E. Eriksson, and H. Martensson, “Balancing efficiency and stability in the design of transonic compressor stages,” *GT2013-94838 ASME Turbo Expo*, 2013.
- [6] DAKOTA (Sandia National Laboratories). <http://www.cs.sandia.gov/DAKOTA/>.
- [7] University of Cincinnati 3DBGB Website <http://qtsl.ase.uc.edu/3DBGB/>.
- [8] K. Siddappaji, M. G. Turner, S. Dey, K. Park, and A. Merchant, “Optimization of a 3-stage booster-part 2: the parametric 3d blade geometry modeling tool,” 2011, ASME Paper Number GT2011-46664.

[9] A. F. Nemnem, M. G. Turner, K. Siddappaji, and M. Galbraith, "A smooth curvature-defined meanline section option for a general turbomachinery geometry generator," GT2014-26363 ASME Turbo Expo, No. GT2014-26363, June 2014.

[10] NUMECA International. FINE/Turbo <http://numeca/>.

[11] S. Drayton, "Design, test, and evaluation of a transonic axial compressor rotor with splitter blades", Ph.D. thesis, NAVAL POSTGRADUATE SCHOOL, September 2013.

[12] "T-axi program," University of Cincinnati T-Axi Website <http://gtsl.ase.uc.edu/T-AXI/>.

[13] K. Siddappaji, M. G. Turner, and A. Merchant, "General capability of parametric 3d blade design tool for turbomachinery," GT2012-69756 ASME Turbo Expo, 2012.

[14] M. G. Turner, A. F. Nemnem, A. J. Gannon, G. V. Hobson, and W. Sanz, "Measured Heat Transfer in a Transonic Fan Rig at Casing With Implications on Performance", GT2015-43482 ASME Turbo Expo, 2015.

[15] G. V. Hobson, A. J. Gannon, and S. Drayton, "Design and Test of A Transonic Axial Splittered Rotor", GT2015-43005 ASME Turbo Expo, 2015.